Supporting Information for

Supramolecular-Confinement Pyrolysis Route to Ultrasmall Rhodium Phosphide Nanoparticles as Robust Electrocatalyst for Hydrogen Evolution at All pH Range and Seawater Electrolysis

Shoujie Liu[b,c#], Yinjuan Chen[a,#], Li Yu[d,#], Yan Lin[a], Zhi Liu[a], Minmin Wang[a], Yanju Chen[a], Chao Zhang[e], Yuan Pan[a,*], Yunqi Liu[a], Chenguang Liu[a]

[a]State Key Laboratory of Heavy Oil Processing, China University of Petroleum (East China), Qingdao, 266580, China

[b]Chemistry and Chemical Engineering of Guangdong Laboratory, Shantou 515063, China

[c]College of Chemistry and Materials Science, Anhui Normal University, Wuhu, Anhui 241000, China

[d]College of Health Science and Environmental Engineering, Shenzhen Technology University, Shenzhen, 518118, China

[e]School of Material Science & Engineering, Tianjin University of Technology, Tianjin 300384, China

[#]These authors contributed equally.

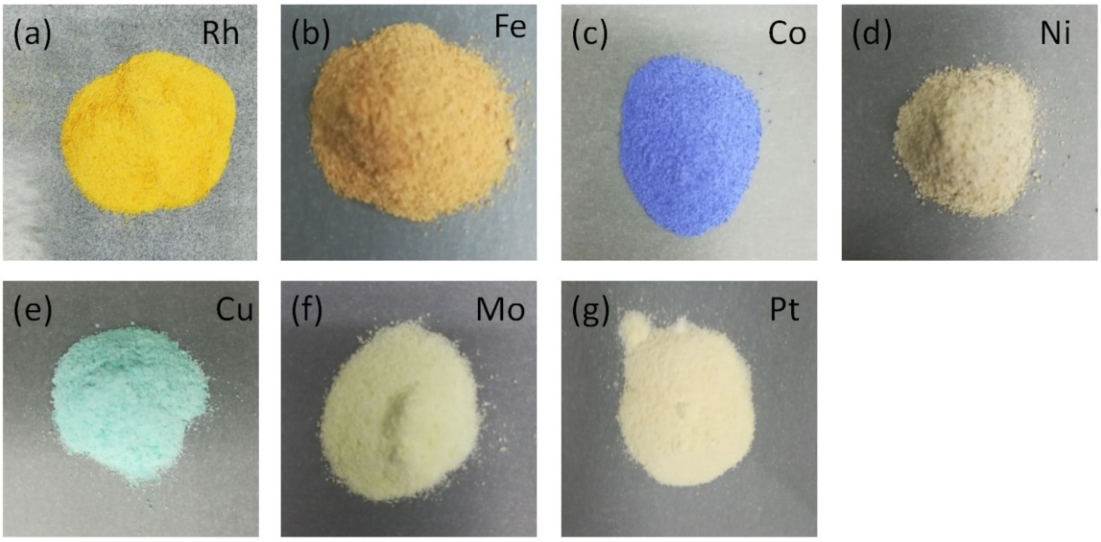

Figure S1. Optical photo images of starch@M-PA precursors.

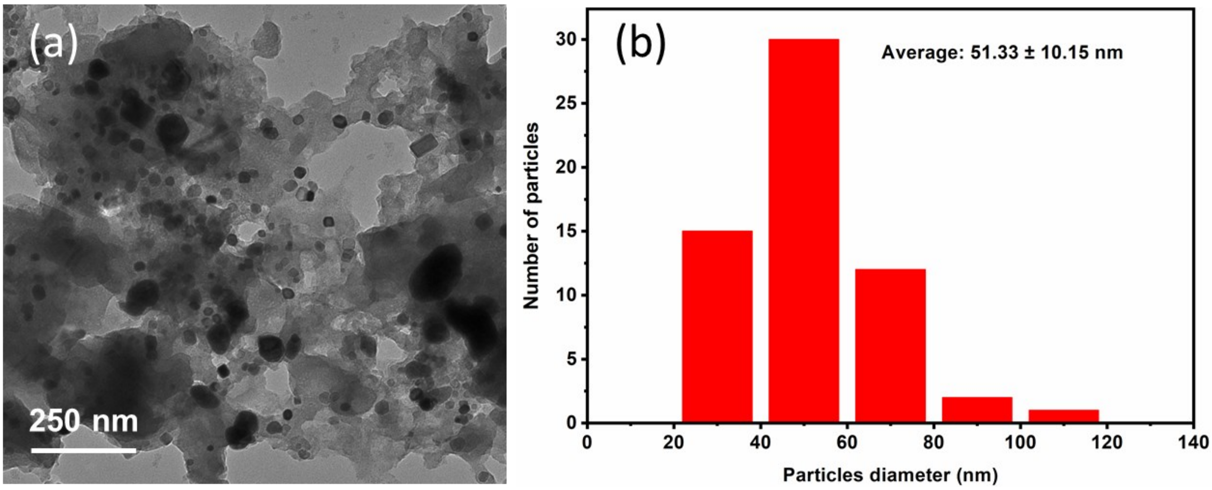

Figure S2. TEM image and size distribution of Rh_2P NPs without the assist of starch.

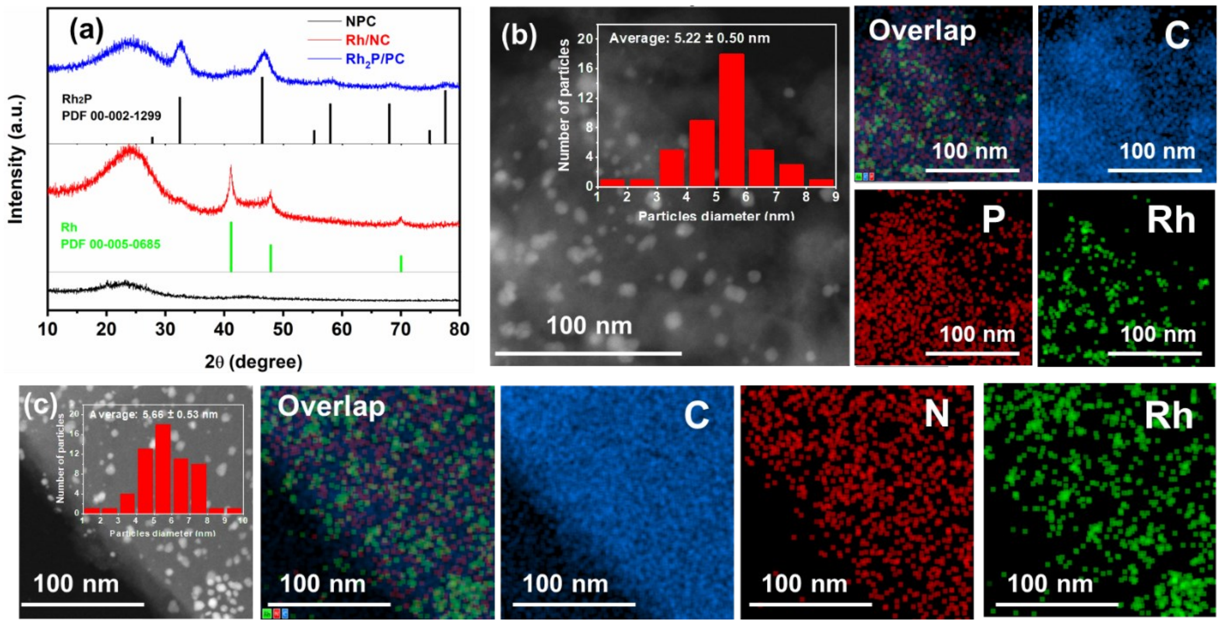

Figure S3. (a) XRD patterns of the Rh_2P/PC, Rh/NC and NPC. HAADF-STEM-EDS mapping images of (b) Rh_2P/PC and (c) Rh/NC. Inset in (b) and (c) show the corresponding size distribution of Rh_2P NPs and Rh NPs.

XRD patterns (Figure S3a) confirmed the cubic Rh_2P phase (PDF No. 00-002-1299, crystal system: cubic, space group: Fm-3m (225), a = 5.516, b = 5.516, c = 5.516) of Rh_2P/PC and the cubic Rh phase (PDF No. 00-005-0685, space group: Fm-3m, a = 3.8031, b = 3.8031, c = 3.8031) of Rh/NC. For the Rh_2P/PC sample, the peaks at 32.5°, 46.7°, 57.9°, 68.1°, and 77.6° can be assigned to the (200), (220), (222), (400) and (420) lattice planes of Rh_2P. For the Rh/NC sample, the peaks at 41.1°, 47.9° and 69.9° can be assigned to the (111), (200) and (220) lattice planes of Rh. All the samples display a broad peak at about 23°, corresponding to the (002) plane of carbon. The average diameter of Rh_2P and Rh NPs is 5.22 ± 0.50 nm (inset of Figure S3b) and 5.66 ± 0.53 nm (inset of Figure S3c). HAADF-STEM-EDS mapping images (Figure S3b) show that C, P, and Rh elements are homogeneously distributed over the entire PC. HAADF-STEM-EDS mapping images (Figure S3c) also show that C, N and Rh elements are homogeneously distributed over the entire NC.

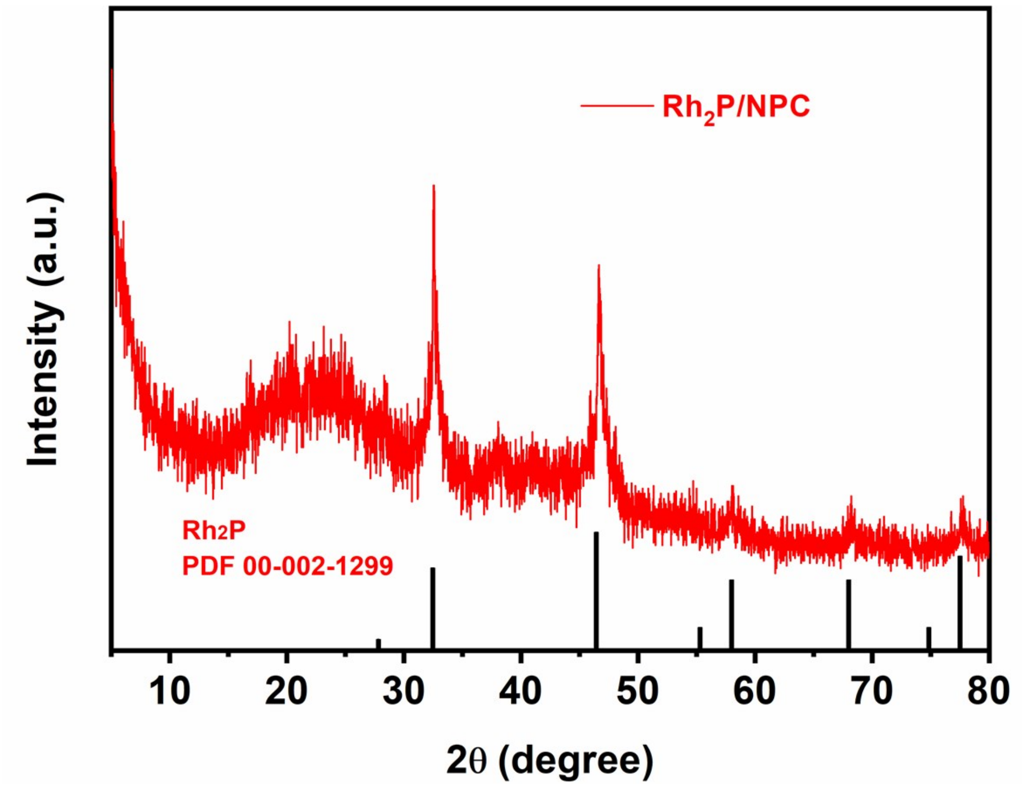

Figure S4. XRD pattern of the Rh_2P/NPC catalyst.

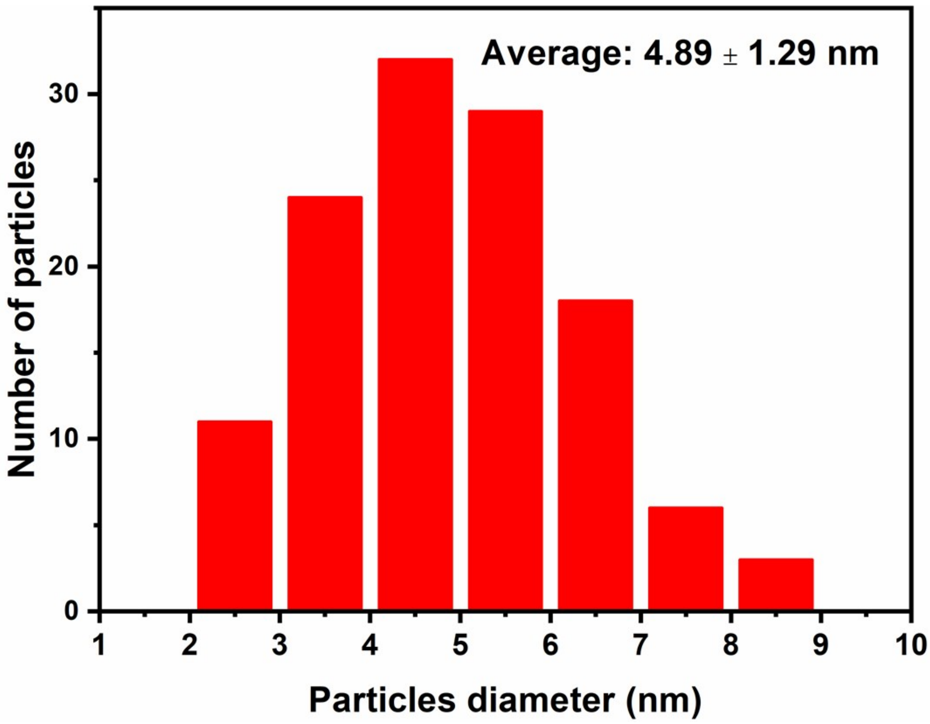

Figure S5. Size distribution of the as-synthesized Rh_2P/NPC catalyst.

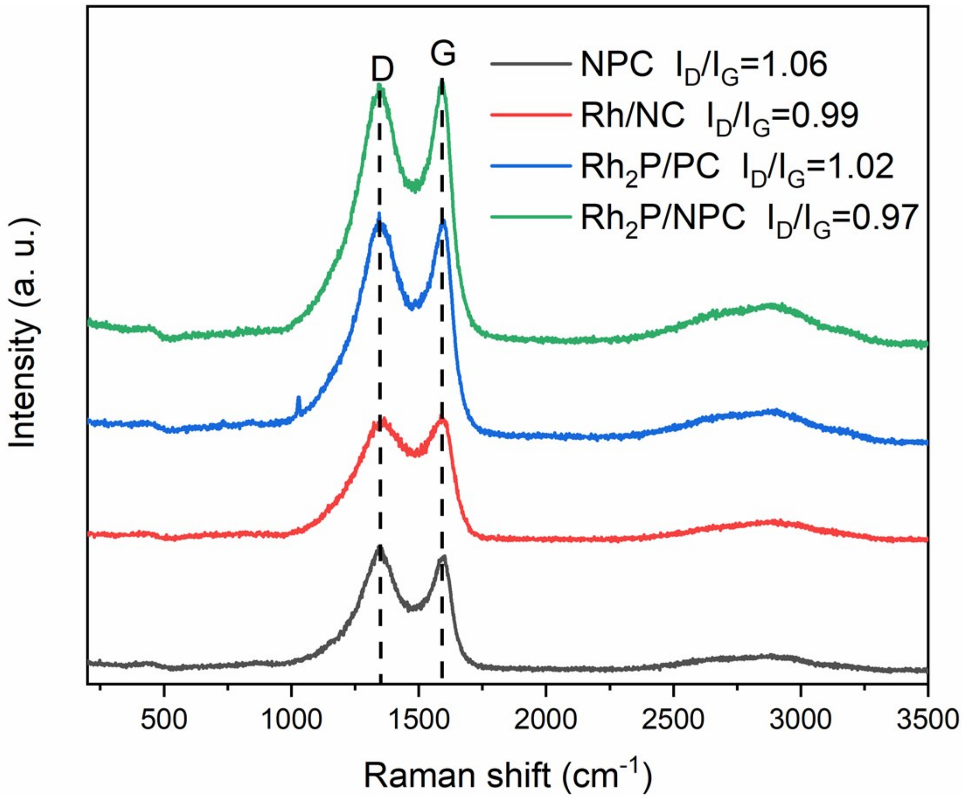

Figure S6. Raman spectra of the as-synthesized Rh_2P/NPC, Rh_2P/PC, Rh/NC and NPC.

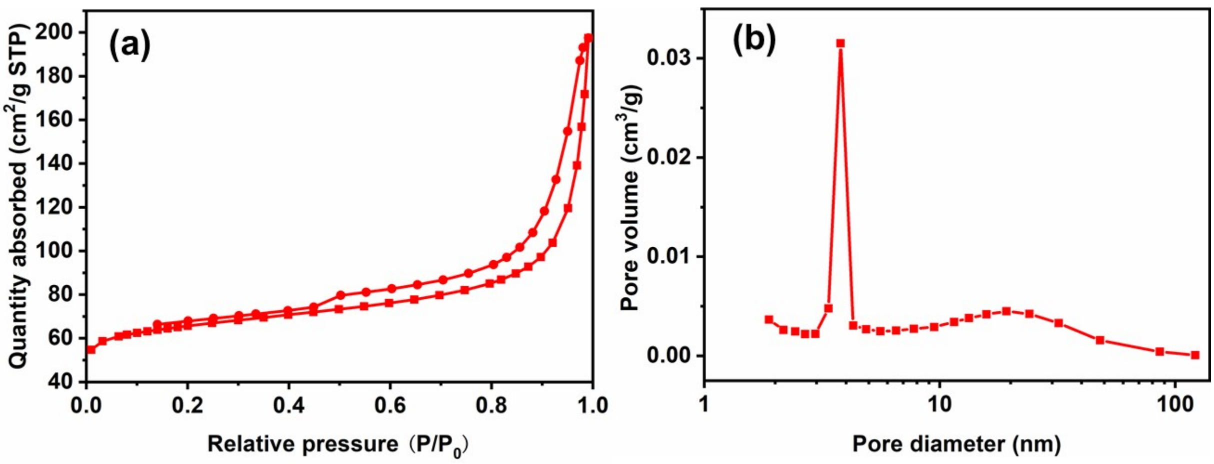

Figure S7. (a) N_2 adsorption-desorption isotherms. (b) porous size distribution curves of Rh_2P/NPC.

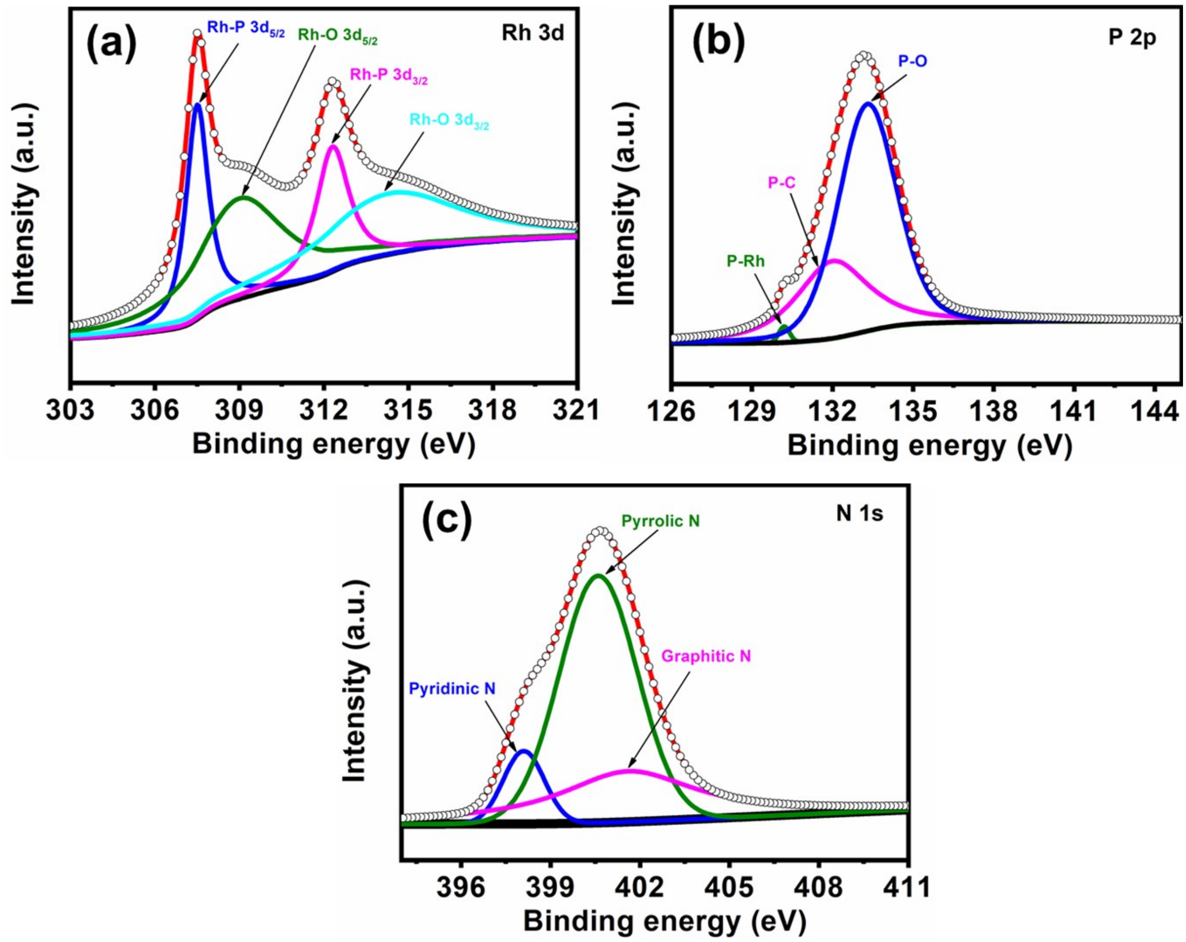

Figure S8. (a) Rh 3d, (b) P 2p, (c) N 1s spectra of the as-synthesized Rh_2P/NPC catalyst.

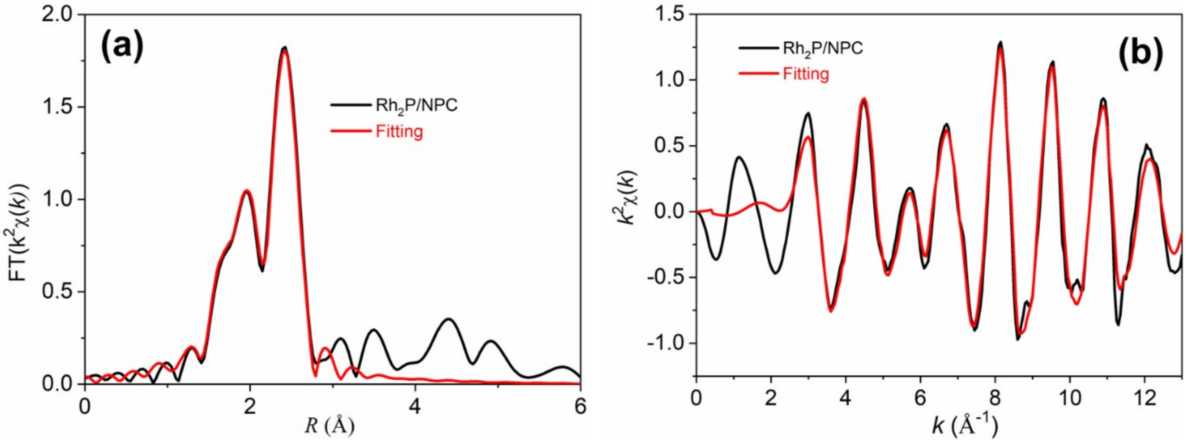

Figure S9. The EXAFS fitting of Rh_2P/NPC at (a) R space and (b) k space.

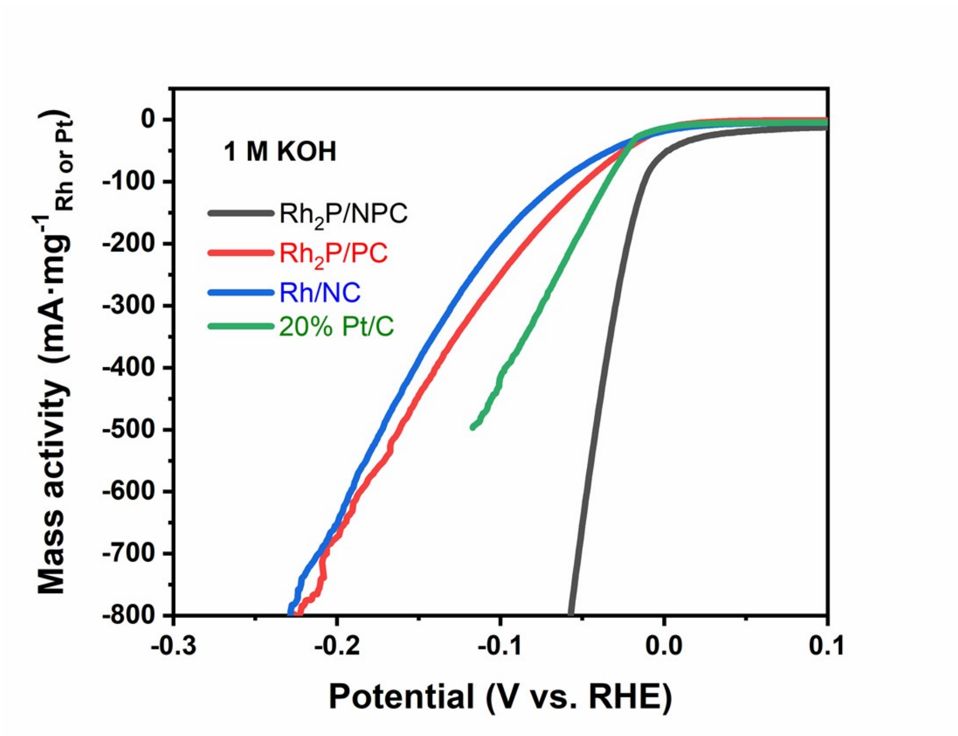

Figure S10. The mass activities of Rh_2P/NPC, Rh_2P/PC, Rh/NC and 20% Pt/C catalysts in 1M KOH.

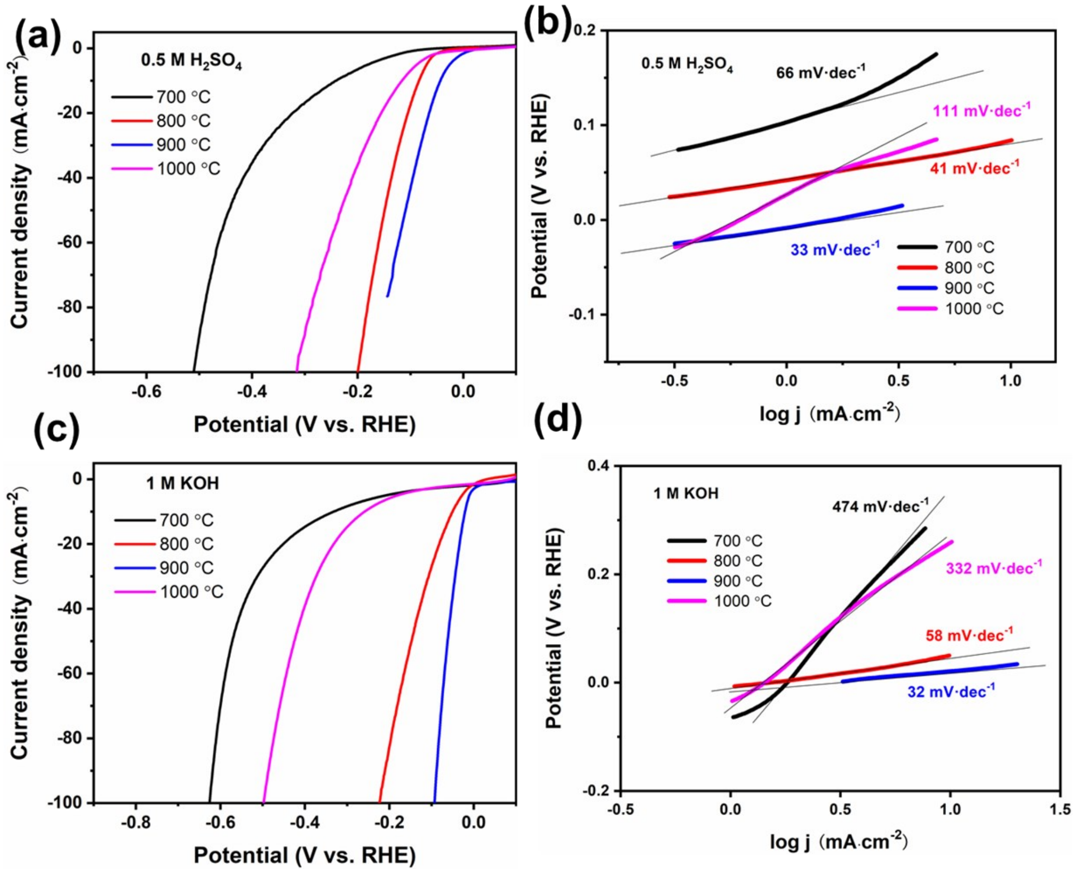

Figure S11. (a, c) LSV curves and (b, d) Tafel plots at different pyrolysis temperature of Rh_2P/NPC catalyst in 0.5 M H_2SO_4 and 1 M KOH, respectively.

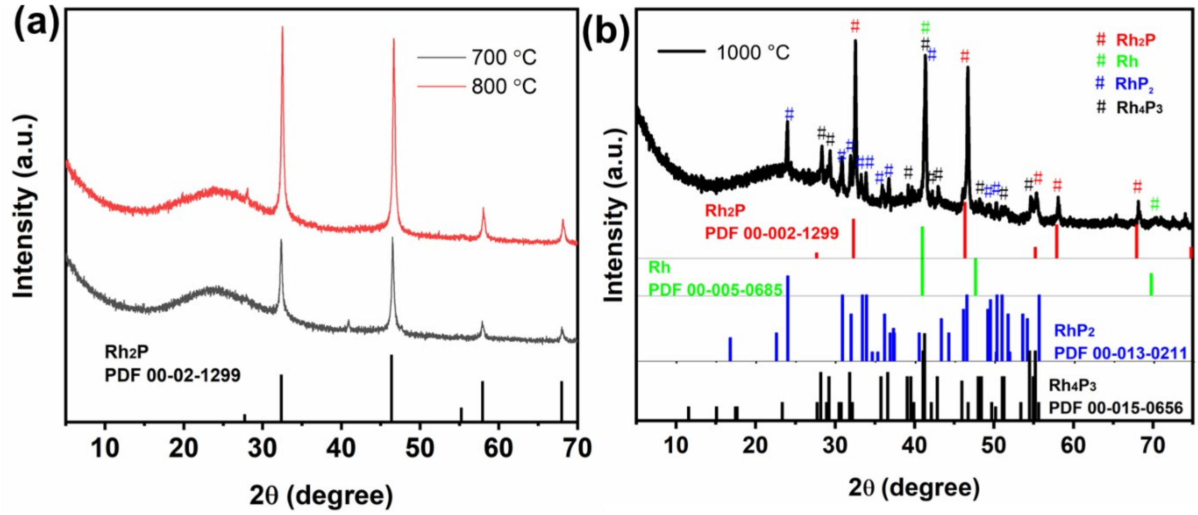

Figure S12. XRD patterns of the products at different pyrolysis temperature of (a) 700 °C, 800 °C and (b) 1000 °C.

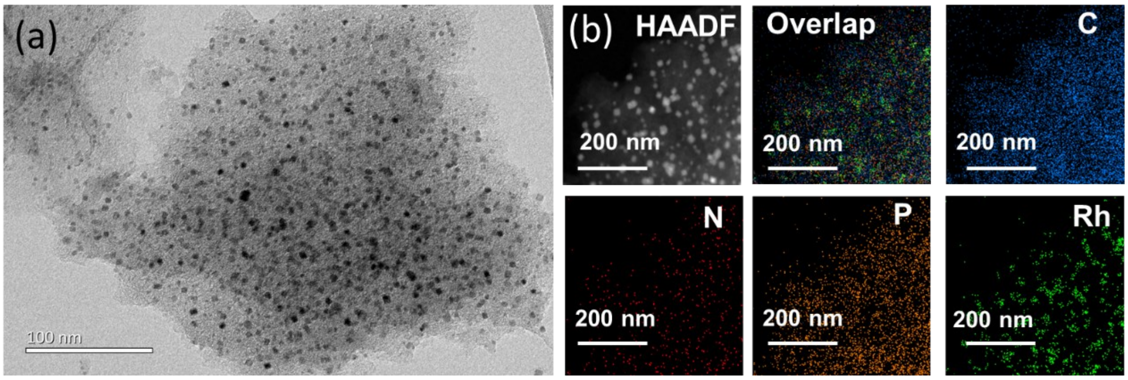

Figure S13. (a) TEM and (b) HADDF-STEM-EDS mapping images of Rh_2P/NPC catalyst after long-term electrolysis in 0.5 M H_2SO_4.

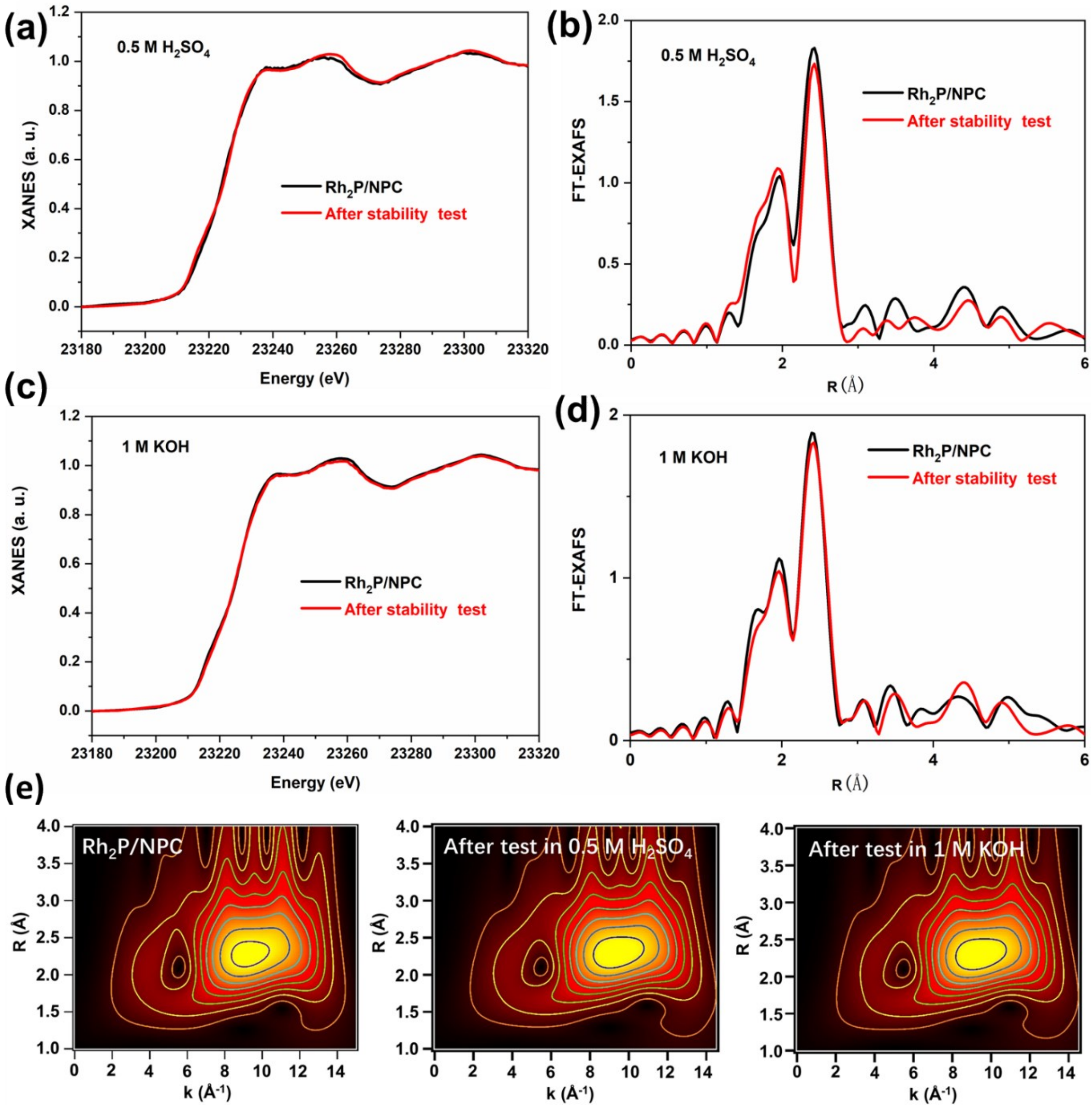

Figure S14. (a, c) XANES and (b, d) FT-EXAFS of Rh_2P/NPC catalyst after long-term electrolysis in 0.5 M H_2SO_4 and 1 M KOH, respectively. (e) WT plots of the Rh_2P/NPC catalyst before and after test in 0.5 M H_2SO_4 and 1 M KOH, respectively.

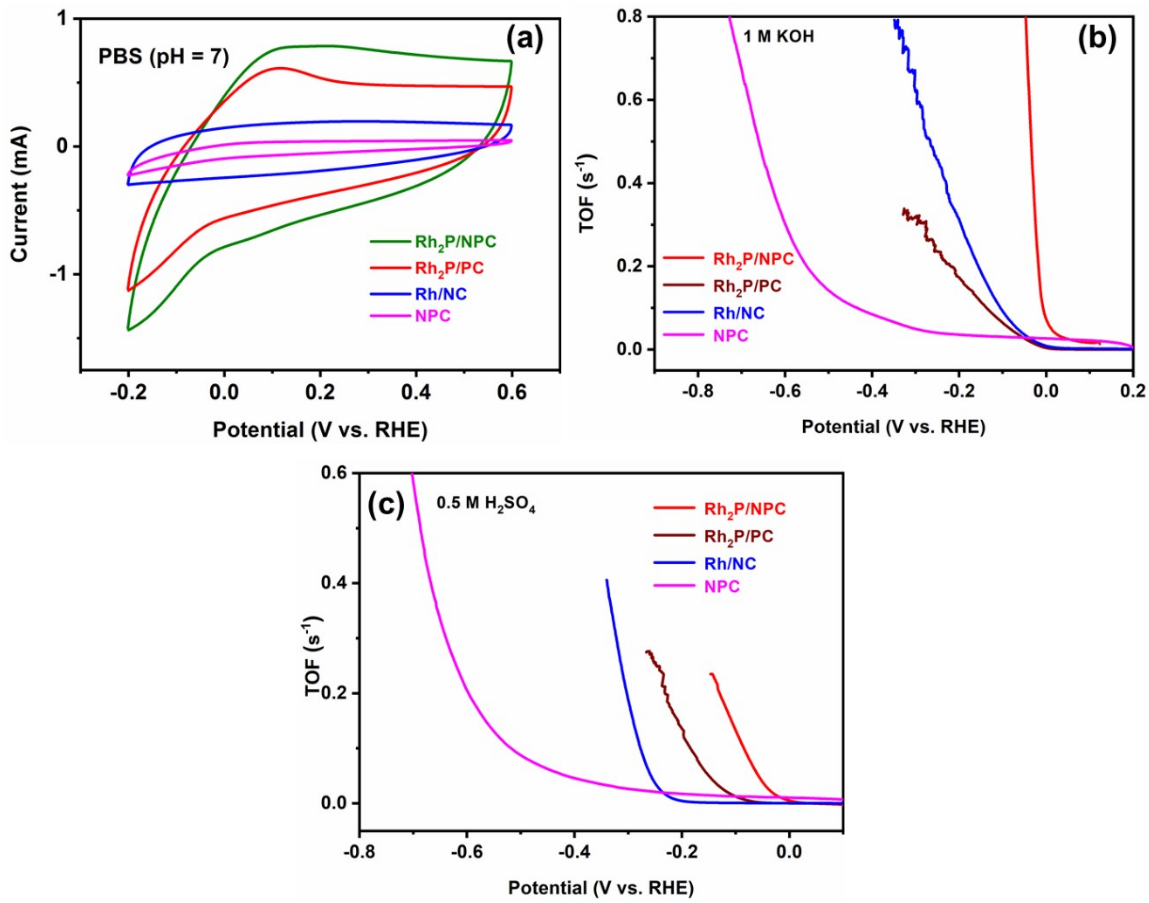

Figure S15. (a) CVs the as-synthesized Rh_2P/NPC, Rh_2P/PC, Rh/NC, and NPC catalysts at pH = 7 with a scan rate of 20 mV·s^{-1}. TOF curves in (b) 1 M KOH and (c) 0.5 M H_2SO_4, respectively.

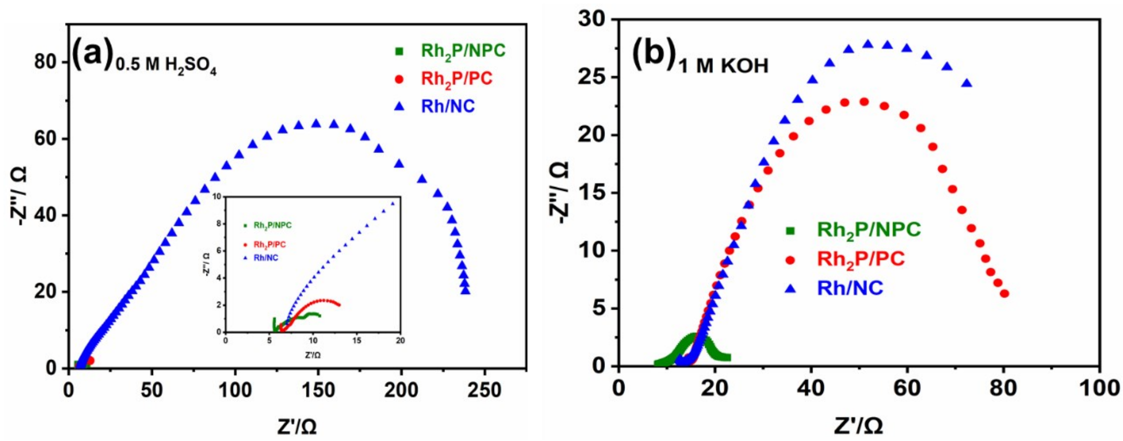

Figure S16. Nyquist plots of the as-synthesized Rh_2P/NPC, Rh_2P/PC, Rh/NC, and NPC catalysts with an overpotential of 180 mV and 80 mV vs. RHE in (a) 0.5 M H_2SO_4 and (b) 1 M KOH, respectively.

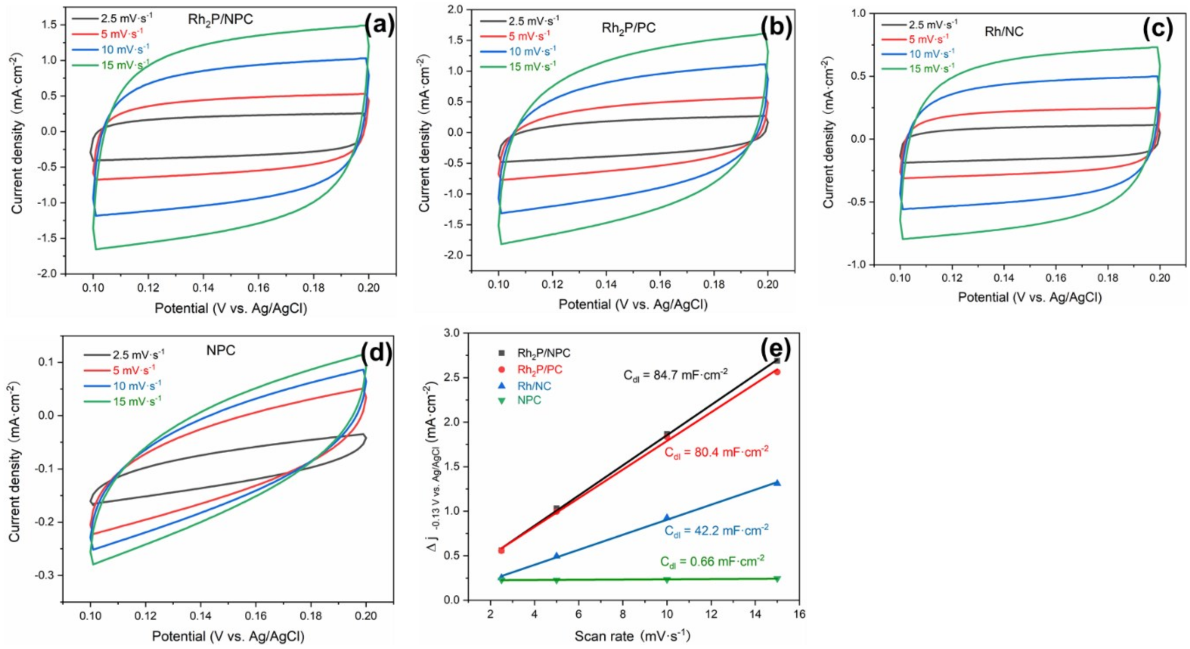

Figure S17. CV curves of the as-synthesized (a) Rh_2P/NPC catalysts, (b) Rh_2P/PC, (c) Rh/NC, and (d) NPC catalysts in 0.5 M H_2SO_4 solution in the region of 0.1~0.2 V vs. Ag/AgCl with different scan rates from 2.5 $mV\cdot s^{-1}$ to 15 $mV\cdot s^{-1}$ for HER.

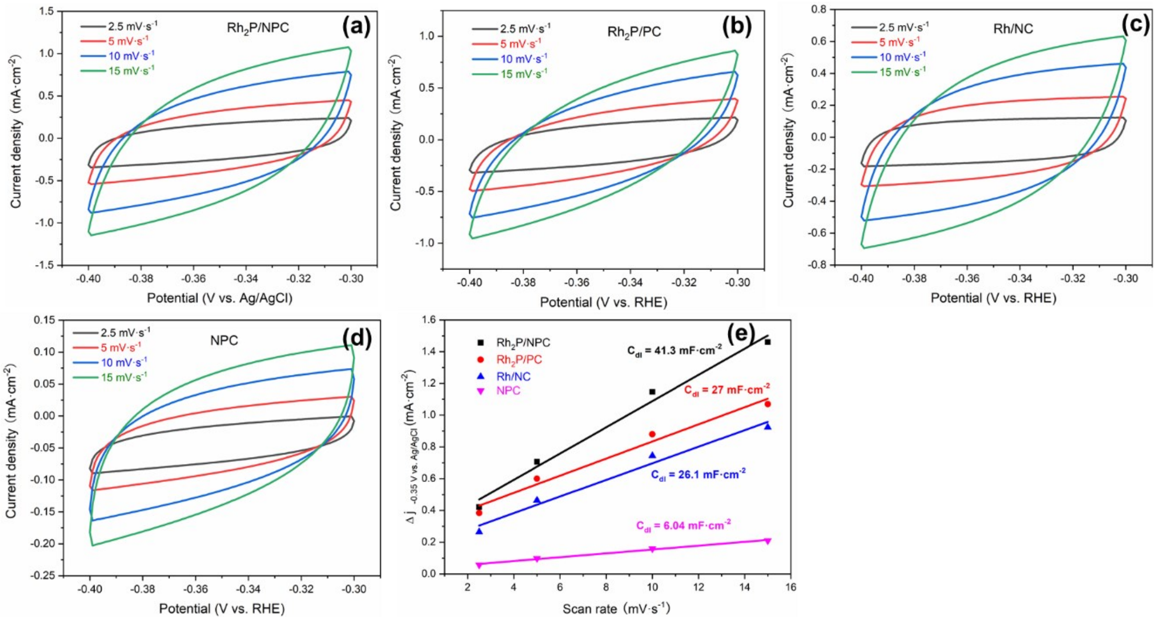

Figure S18. CV curves of the as-synthesized (a) Rh_2P/NPC catalysts, (b) Rh_2P/PC, (c) Rh/NC, and (d) NPC catalysts in 1 M KOH solution in the region of -0.4~-0.3 V vs. Ag/AgCl with different scan rates from 2.5 $mV{\cdot}s^{-1}$ to 15 $mV{\cdot}s^{-1}$ for HER.

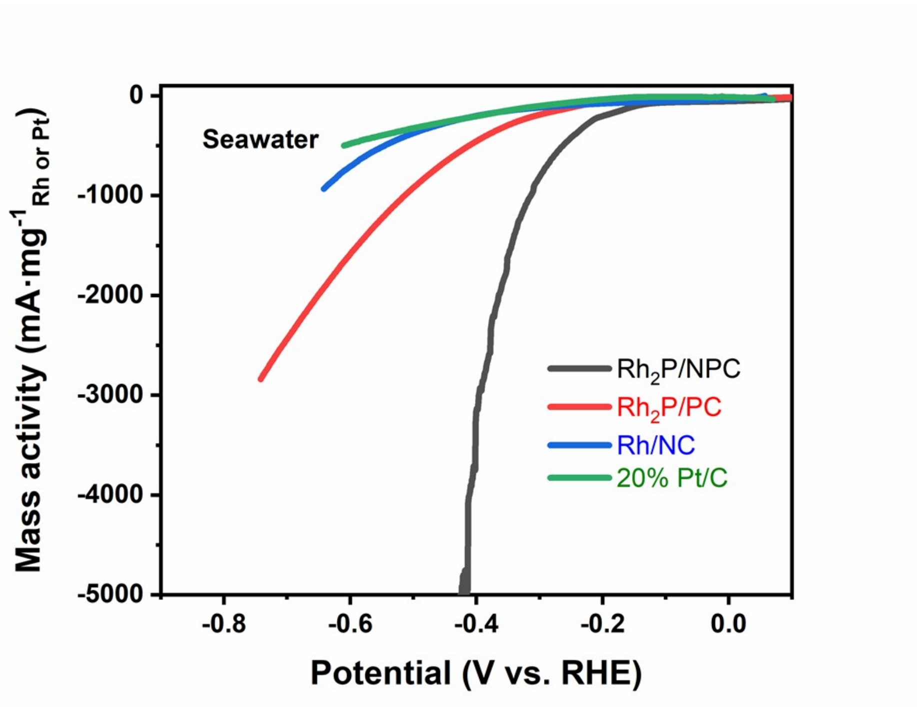

Figure S19. The mass activities of Rh_2P/NPC, Rh_2P/PC, Rh/NC and 20% Pt/C catalysts in natural seawater.

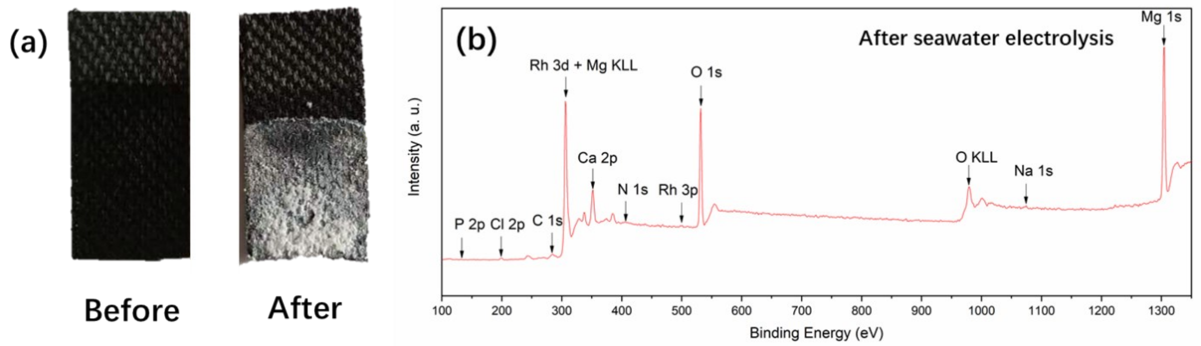

Figure S20. (a) Optical images of the Rh_2P/NPC catalyst before and after seawater electrolysis. (b) XPS survey spectrum of the Rh_2P/NPC catalyst after seawater electrolysis.

In Figure S20(a), the optical images of the Rh_2P/NPC catalyst sample clearly show that there are some white insoluble precipitates covering the catalyst surface after seawater electrolysis. In Figure S20(b), the XPS analysis further confirmed the precipitates are mainly comprised of Na, Ca and Mg salts, which are the typical components of natural seawater.

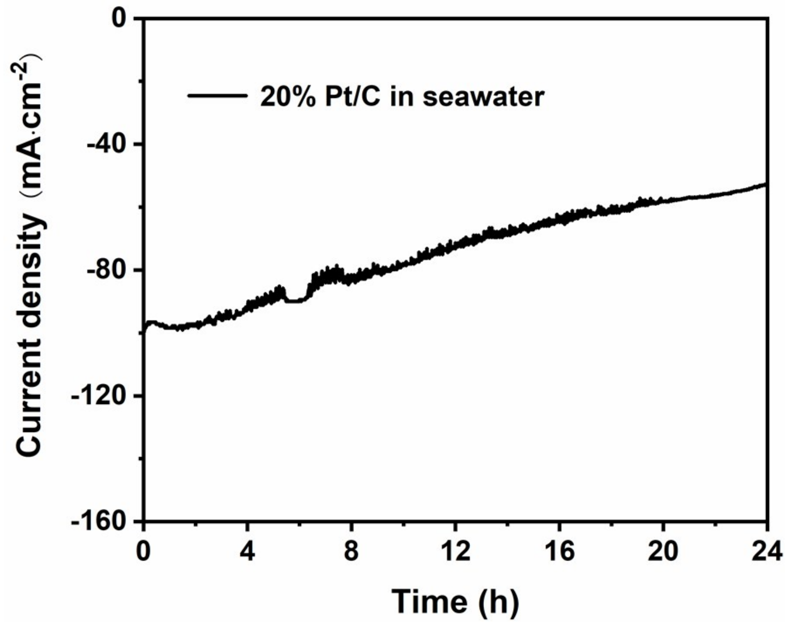

Figure S21. Time-dependent current density curves of the 20% Pt/C catalyst at -0.6 V vs. RHE in natural seawater.

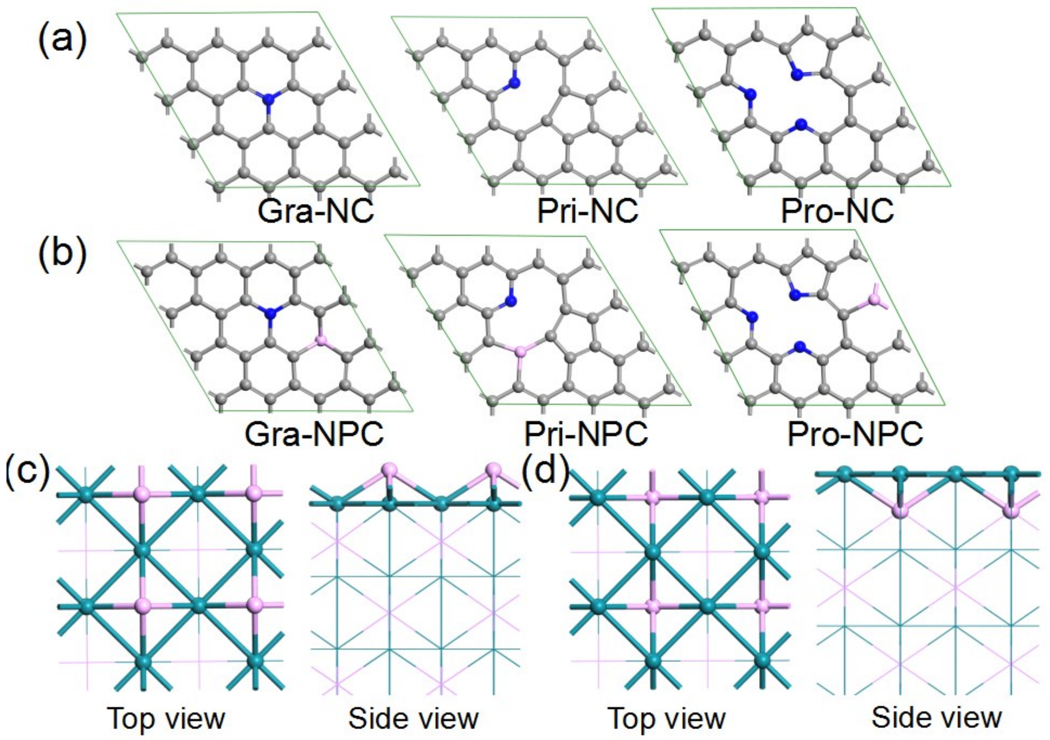

Figure S22. Optimized geometry configurations. (a) Modelized N-doped porous carbon (NC) and N, P co-doped porous carbon (NPC), here Gra-, Pri- and Pro- denote graphitic, pyridinic and pyrrolic materials, respectively). Optimized structures of (c) P terminated and (d) Rh terminated Rh_2P (200) surface.

According to the aforementioned heteroatom's chemical environments obtained from the XPS spectra, graphitic, pyrrolic, and pyridinic N doped graphene sheets were built to simulate the NC. On the base of N, C moieties, the NPC was modeled with one C atom replaced by P atom at the position along the graphene where the P atom is departed from the specific N atoms with two C atoms. In which, the link bonds are agree with the C K-edge result that C-N-C and C-P-C defect sites are coexisted in the carbon lattice. To further explain the synergistic effects that originated from Rh_2P NPs and NPC, a slab with P doped pyridinic NC (Pri-NPC) anchored on the P-terminated Rh_2P was used, since the N site on Pri-NPC and the P site on P-terminated Rh_2P performed the relatively outstanding HER activity among the catalysts mentioned above.

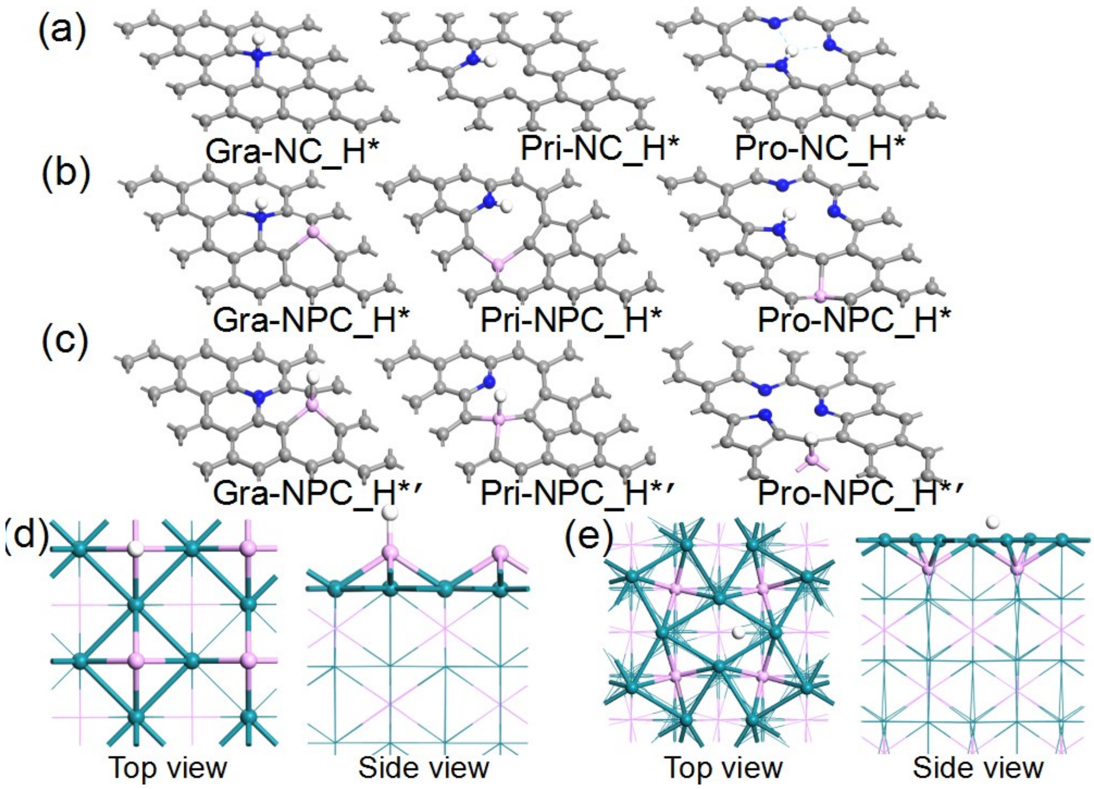

Figure S23. Optimized geometry configurations of the hydrogen adsorbed moieties, (a) for NC, (b) for the N site of NPC and (c) for the P site of NPC. (d) H adsorption structures on P terminated and (e) Rh terminated Rh_2P.

Graphitic, pyrrolic, and pyridinic N doped graphene sheets (Gra-NC, Pro-NC and Pri-NC, respectively) with one hydrogen atom adhered on the characteristic N sites were taken into consideration to reveal the effect of N doped carbon on HER activity.

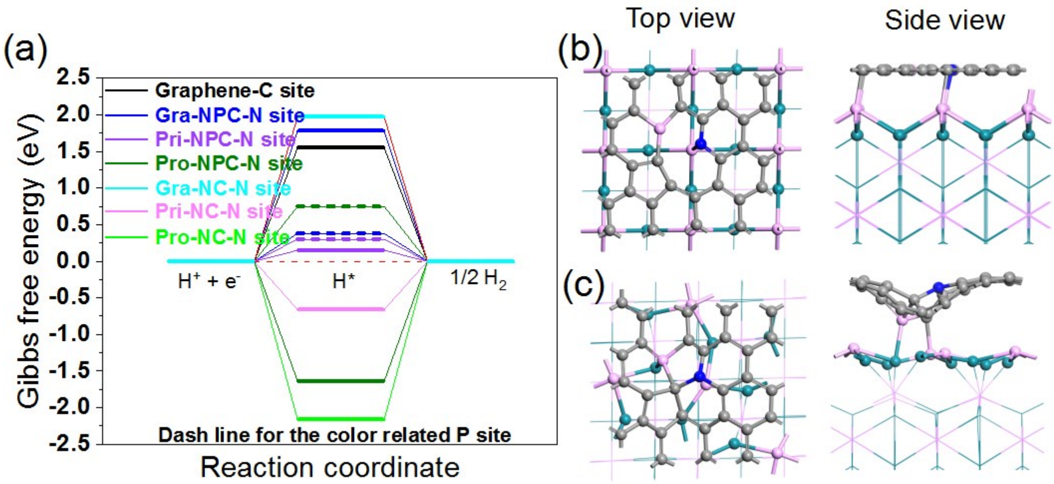

Figure S24. HER mechanism. (a) Gibbs free-energy diagrams for HER on NPC and NC. The dash line represents for the color related P site. Initial geometry configurations of (b) Rh_2P/NPC and (c) optimized structures of Rh_2P/NPC.

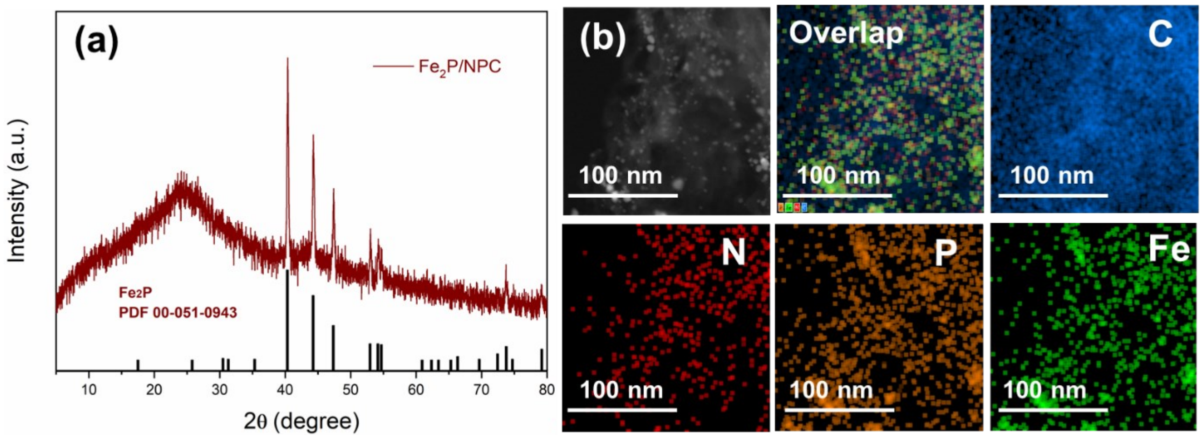

Figure S25. (a) XRD pattern and (b) HAADF-STEM-EDS mapping images of Fe_2P/NPC.

XRD pattern (Figure S22a) confirms the hexagonal Fe_2P phase (PDF No. 00-051-0943, space group: P-62m, a = 5.8685, b = 5.8685, c = 3.4571). The peaks at 40.4°, 44.3°, 47.4°, 52.9°, 54.2°, and 73.7° can be assigned to the (111), (201), (210), (002), (300) and (212) lattice planes of Fe_2P. HAADF-STEM-EDS mapping images (Figure S22b) show that all the elements including C, N, P, and Fe are homogeneously distributed over the entire NPC.

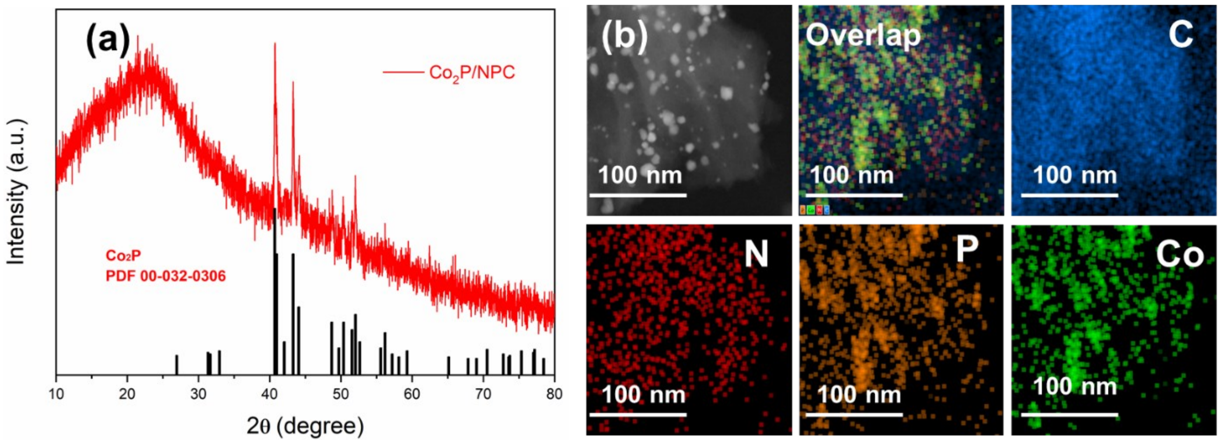

Figure S26. (a) XRD pattern and (b) HAADF-STEM-EDS mapping images of Co_2P/NPC.

XRD pattern (Figure S23a) confirms the orthorhombic Co_2P phase (PDF No. 00-032-0306, space group: Pnam, a = 5.6465, b = 6.6099, c = 3.5130). The peaks at 40.7°, 43.3°, 44.2°, 48.7°, 50.3°, 51.5°, 52.1° and 56.3° can be assigned to the (121), (211), (130), (031), (310), (131), (002) and (320) lattice planes of Co_2P. HAADF-STEM-EDS mapping images (Figure S23b) show that all the elements including C, N, P, and Co are homogeneously distributed over the entire NPC.

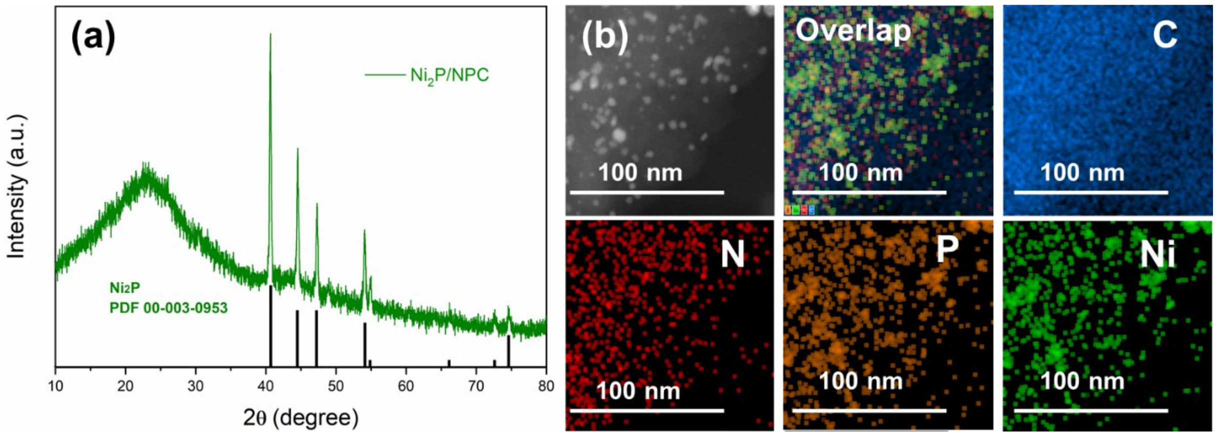

Figure S27. (a) XRD pattern and (b) HAADF-STEM-EDS mapping images of Ni_2P/NPC.

XRD pattern (Figure S24a) confirms the hexagonal Ni_2P phase (PDF No. 00-003-0953, space group: P321, a = 5.86, b = 5.86, c = 3.37). The peaks at 40.7°, 44.5°, 47.2°, 54.1°, 54.9°, 66.2°, 72.7° and 74.7° can be assigned to the (111), (201), (210), (300), (211), (310), (311) and (400) lattice planes of Ni_2P. HAADF-STEM-EDS mapping images (Figure S24b) show that all the elements including C, N, P, and Ni are homogeneously distributed over the entire NPC.

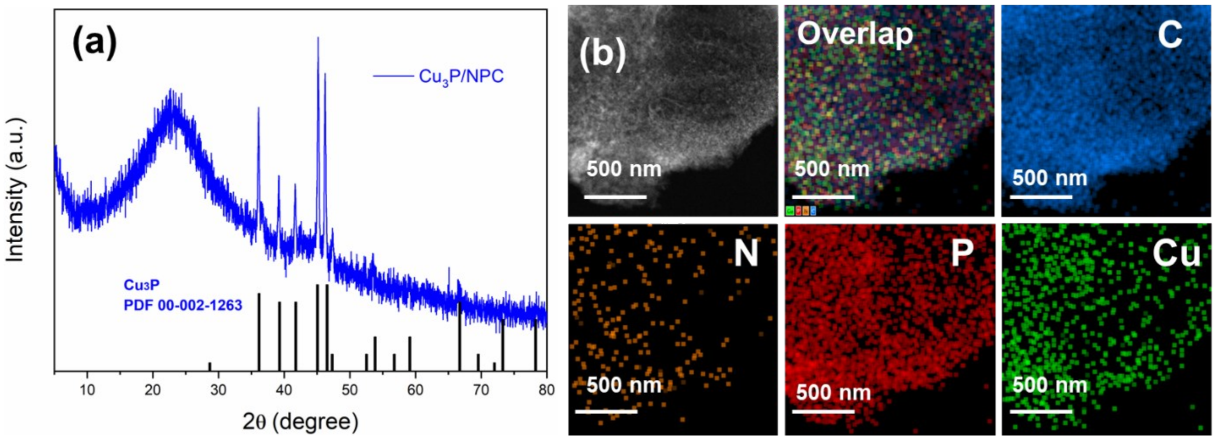

Figure S28. (a) XRD pattern and (b) HAADF-STEM-EDS mapping images of Cu_3P/NPC.

XRD pattern (Figure S25a) confirms the hexagonal Cu_3P phase (PDF No. 00-002-1263, space group: P-3c1, a = 6.954, b = 6.954, c = 7.149). The peaks at 36.1°, 39.1°, 41.7°, 45.2°, 46.2°, 47.4°, 52.2°, 53.5° and 66.6° can be assigned to the (112), (202), (211), (300), (113), (212), (220), (221) and (223) lattice planes of Cu_3P. HAADF-STEM-EDS mapping images (Figure S25b) show that all the elements including C, N, P, and Cu are homogeneously distributed over the entire NPC.

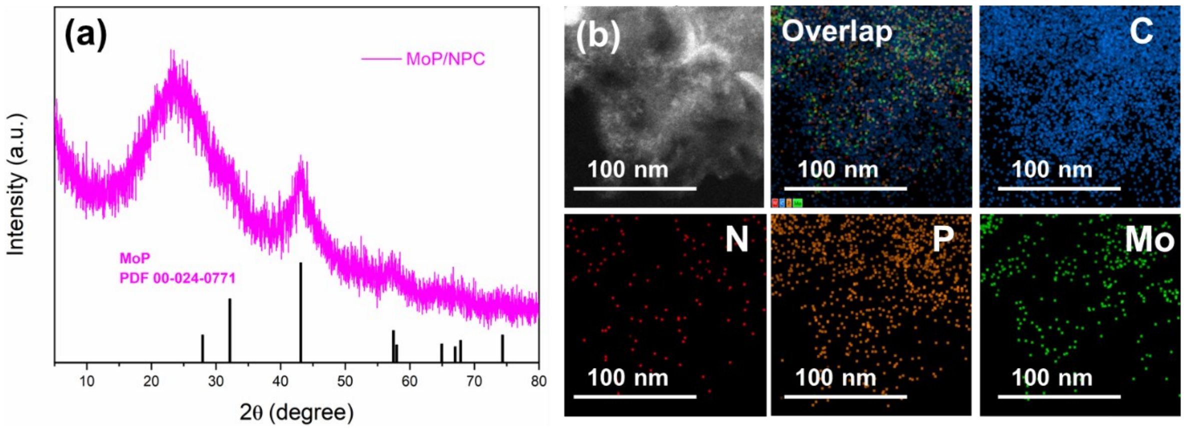

Figure S29. (a) XRD pattern and (b) HAADF-STEM-EDS mapping images of MoP/NPC.

XRD pattern (Figure S26a) confirms the hexagonal MoP phase (PDF No. 00-024-0771, space group: P-6m2, a = 3.222, b = 3.222, c = 3.191). The peaks at 43.1° and 57.2°can be assigned to the (101) and (110) lattice planes of MoP. HAADF-STEM-EDS mapping images (Figure S26b) show that all the elements including C, N, P, and Mo are homogeneously distributed over the entire NPC.

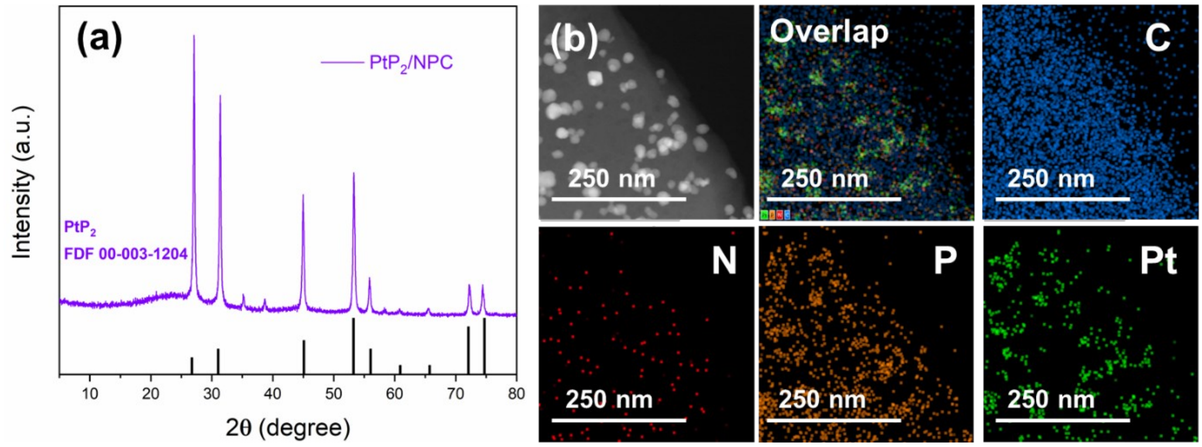

Figure S30. (a) XRD pattern and (b) HAADF-STEM-EDS mapping images of PtP_2/NPC.

XRD pattern (Figure S27a) confirms the cubic PtP_2 phase (PDF No. 00-003-1204, space group: Pa-3, a = 5.7, b = 5.7, c = 5.7). The peaks at 26.9°, 31.1°, 44.9°, 53.4°, 56.0°, 60.7°, 65.5°, 72.1° and 74.4° can be assigned to the (111), (200), (220), (311), (222), (321), (400), (331) and (420) lattice planes of PtP_2. The small peaks at 35.2°, 38.8° and 58.3° may be impurity peaks. The HAADF-STEM-EDS mapping images (Figure S27b) show that all the elements including C, N, P, and Pt are homogeneously distributed over the entire NPC.

Table S1. Structural parameters of the Rh foil, Rh_2O_3 and Rh_2P/NPC extracted from the EXAFS fitting. (S_0^2=0.80).

Sample	Shell	N	R_j(Å)	σ^2 (10^{-3}Å^2)	ΔE_0 (eV)
Rh foil	Rh-Rh	12	2.71	3	4.1
Rh_2O_3	Rh-O	6	2.03	4.8	-3.0
	Rh-Rh1	1	2.71	4.9	-3.5
	Rh-Rh2	3	2.98	4.9	-3.5
Rh_2P/NPC	Rh-P	4.0	2.34	6.2	-2.7
	Rh-Rh	5.7	2.75	6.5	3.9

Table S2. Calculated adsorption energies and Gibbs free energies of H adsorbed on the related catalysts.

Binding site	Adsorption energy, E_{ads} /eV	Adsorption free energy, ΔG_H/ EV
Gra-NC-N	1.80	1.97
Pro-NC-N	-2.69	-2.16
Pri-NC-N	-1.09	-0.66
Gra-NPC-N	1.62	1.78
Pro-NPC-N	-1.80	-1.64
Pri-NPC-N	-0.05	0.15
Gra-NPC-P	0.22	0.38
Pro-NPC-P	0.00	0.75
Pri-NPC-P	0.10	0.30
Rh_2P-P-terminated	-0.09	0.26
Rh_2P-Rh-terminated	-2.76	-1.83
Rh_2P/NPC-N	1.31	1.47
Rh_2P/NPC-P	-0.07	-0.06